Research article

An analytical model describing the mechanics of erythrocyte membrane wrapping during active invasion of a plasmodium falciparum merozoite

Chimwemwe Msosa[1,2,*], Tamer Abdalrahman[1,3], Thomas Franz[1,4]

[1]Division of Biomedical Engineering, Department of Human Biology, University of Cape Town, Observatory 7925, South Africa

[2]Faculty of Engineering, Department of Electrical Engineering, Malawi University of Business and Applied Sciences, Blantyre, Malawi

[3]Computational Mechanobiology, Julius Wolff Institute for Biomechanics and Musculoskeletal Regeneration, Charité Universitätsmedizin, Berlin 13353, Germany

[4]Bioengineering Science Research Group, Engineering Sciences, Faculty of Engineering and Physical Sciences, University of Southampton, Southampton SO171BJ, UK

* Corresponding author: cmsosa@poly.ac.mw

ORCID

Chimwemwe Msosa: 0000-0003-1021-9308

Tamer Abdalrahman: 0000-0002-0320-811X

Thomas Franz: 0000-0002-1504-3842

Abstract

The invasion of a merozoite into an erythrocyte by membrane wrapping is a hallmark of malaria pathogenesis. The invasion involves biomechanical interactions whereby the merozoite exerts actomyosin-based forces to push itself into and through the erythrocyte membrane while concurrently inducing biochemical damage to the erythrocyte membrane. Whereas the biochemical damage process has been investigated, the detailed mechanistic understanding of the invasion mechanics remains limited. Thus, the current study aimed to develop a mathematical model describing the mechanical factors involved in the merozoite invasion into an erythrocyte and explore the invasion mechanics.

A shell theory model was developed comprising constitutive, equilibrium and governing equations of the deformable erythrocyte membrane to predict membrane mechanics during the wrapping of an entire non-deformable ellipsoidal merozoite. Predicted parameters include principal erythrocyte membrane deformations and stresses, wrapping and indentation forces, and indentation work. The numerical investigations considered two limits for the erythrocyte membrane deformation during wrapping (4% and 51% areal strain) and erythrocyte membrane phosphorylation (decrease of membrane elastic modulus from 1 to 0.5 kPa).

For an intact erythrocyte, the maximum indentation force was 1 and 8.5 pN, and the indentation work was 1.92×10^{-18} and 1.40×10^{-17} J for 4% and 51% areal membrane strain. Phosphorylation damage in the erythrocyte membrane reduced the required indentation work by 50% to 0.97×10^{-18} and 0.70×10^{-17} J for 4% and 51% areal strain.

The current study demonstrated the developed model's feasibility to provide new knowledge on the physical mechanisms of the merozoite invasion process that contribute to the invasion efficiency towards the discovery of new invasion-blocking anti-malaria drugs.

Keywords: malaria; red blood cell; phosphorylation; spectrin network; mathematical model;

Nomenclature

A_0	Undeformed erythrocyte membrane area
A_p	Projected erythrocyte membrane area
A_s	Areal strain of the erythrocyte membrane
$A_{s,max}$	Maximum areal strain of the erythrocyte membrane
A_w	Wrapped surface area of the merozoite
$\check{A}$	3D merozoite shape parameter
c	Stretch parameter
C_{01}	Material parameter
C_{10}	Material parameter
d_i	Indentation depth
E	Elastic modulus
E_i	Parasite indentation work
$\check{E}$	3D merozoite shape parameter
e_s	Shear strain
F_i	Parasite indentation force
F_w	Parasite wrapping force
G_s	Shear modulus
$\check{G}$	3D merozoite shape parameter
h_t	Erythrocyte membrane thickness
I_1	First strain invariant
I_2	Second strain invariant
k_1	Meridian curvature
k_2	Circumferential curvature
m	Stretch parameter
M_c	Coverage area of the erythrocyte membrane
MR-T_1	Meridian tension obtained using the Mooney Rivlin law
MR-T_2	Circumferential tension obtained using the Mooney Rivlin law
n	Stretch parameter
P	Pressure acting on the erythrocyte surface

R_a	Merozoite shape parameter
R_b	Merozoite shape parameter
T_1	Principal meridian tension
T_2	Principal circumferential tension
x	x coordinate of a point on the merozoite surface
y	y coordinate of a point on the merozoite surface
z	z coordinate of a point on the merozoite surface
β	Ratio of material parameters
Γ	Linear coverage of the erythrocyte membrane
Γ_c	Arch length on the merozoite surface
θ	Polar angle defining the merozoite shape
λ_1	Principal meridian stretch
$\lambda_{1,max}$	Maximum principal meridian stretch
λ_2	Principal circumferential stretch
$\lambda_{2,max}$	Maximum principal circumferential stretch
μ	Dynamic viscosity
μ_0	Initial shear modulus
μ_s	Shear stress
ν	Poisson's ratio
ρ	Polar coordinate point on the merozoite surface
ρ_0	Initial polar coordinate of a point on the merozoite surface at which the tight junction forms
σ_1	Principal meridian stress
σ_2	Principal circumferential stress
Ψ	Mooney Rivlin strain energy density function per reference volume
φ	Polar angle defining the merozoite shape

1 Introduction

The invasion of malaria merozoites into erythrocytes marks the pathogenesis of malaria. The invasion process involves mechanical and biochemical interactions to optimise the invasion efficiency. The wrapping of the merozoite by the erythrocyte membrane begins with a low-affinity attachment of the merozoite on the surface of the erythrocyte membrane, followed by a cascade of key events, i.e. the active entry in which the merozoite exerts an actomyosin force, the induction of erythrocyte membrane skeleton remodelling, the establishment of a tight junction between merozoite and erythrocyte membrane, and the sealing of the erythrocyte membrane.

The role of molecular factors in human erythrocyte invasion by a merozoite has been extensively investigated (Cowman and Crabb, 2006). However, identifying antimalarial compounds that target the merozoite binding during the entry has been a significant challenge. The reason is the redundancy of erythrocyte membrane proteins; it is impossible to block the erythrocyte invasion unless all surface proteins are disrupted. New approaches in proteomics (Guiguemde et al., 2010), chemoinformatics (Plouffe et al., 2008), and genetics (Rottmann et al., 2010) have shown promise in addressing this challenge. Nevertheless, a vaccine blocking the merozoite invasion is unavailable for clinical use due to limited knowledge of the invasion process.

Mechanistic research into erythrocyte invasion by merozoites is very scarce. An *in vitro* study by Li et al. (2014) into the invasion mechanics indicated that the yield point in quasi-statically loaded erythrocyte membranes ranged between 2% and 4% areal strain, beyond which lysis of the erythrocyte was observed. Dasgupta et al. (2014) developed a mathematical model of the erythrocyte membrane wrapping and predicted the contribution of wrapping to the invasion energetics. Abdalrahman and Franz (2017) proposed an analytical model based on contact mechanics to describe the erythrocyte membrane deformation due to the ligand-receptor adhesion energy released during membrane indentation up to 10% of the merozoite length.

Mechanical markers, also referred to as mechanical phenotypes or mechanotypes, are emerging label-free markers that may offer the potential for use as drug targets (Qi et al., 2015). However, the poor mechanobiological understanding of the merozoite invasion process has limited the scope of anti-malaria drug targets.

Mathematical and computational investigations can clarify the mechanisms that determine the merozoite's invasiveness and contribute to developing novel invasion blocking antimalarial compounds. As a first step, a detailed mathematical description of the biomechanical interactions between merozoite and erythrocyte during the invasion process is required.

Hence, this study aimed to develop an analytically model that describes the erythrocyte membrane mechanics during the entire merozoite entry and investigate with the model the effects of erythrocyte membrane deformation and phosphorylation on invasion forces and work.

2 Methods

The erythrocyte membrane wrapping mechanism was described analytically using the membrane theory of shells. A differential equation describing the equilibrium configuration of a circular erythrocyte membrane section and a rigid egg-shaped merozoite was solved numerically throughout the entire invasion process (Villaggio, 1997). The deformation of the erythrocyte membrane was described using merozoite shape parameters. Equilibrium and governing equations were formulated with deformation and constitutive law of the erythrocyte. The governing equations were numerically solved using the Runge Kutta fourth-order method to obtain stretches and stresses in the erythrocyte membrane.

The erythrocyte membrane wrapping mechanics was explored for two values of areal erythrocyte membrane strain, i.e. $A_s \leq 4\%$ as generally accepted for quasi-static erythrocyte membrane deformation (Li et al., 2013) and $A_s \leq 51\%$. Additionally, the impact of the tight junction and merozoite-induced erythrocyte membrane damage on the invasion energetics were considered.

The following simplifying assumptions were used for the wrapping mechanics of a health erythrocyte during merozoite entry:

a) The erythrocyte membrane is homogeneous and mechanically isotropic.
b) The erythrocyte membrane has a small thickness of 0.01 µm.
c) The region of the erythrocyte membrane involved in the wrapping is initially flat.
d) The bending modulus of the erythrocyte membrane is small, and only the mid-plane strain due to loading modes other than bending is considered.
e) The merozoite is rigid, i.e., non-deformable.

2.1 Physical properties of an erythrocyte

A healthy mature human erythrocyte is a biconcave discoid shaped cell with a diameter of 7.8 µm and a thickness that varies from 0.8 to 2.6 µm. It is mainly composed of the cytoplasm surrounded by a membrane. In a healthy erythrocyte, the cytoplasm comprises a concentrated haemoglobin solution with a viscosity of approximately 6 to 10 mPa s (Dimitrakopoulos, 2012). Under normal physiological conditions, the haemoglobin viscosity has a negligible contribution to erythrocyte deformability, mainly determined by its membrane. However, at high viscosity of 650 mPa s (Mohandas and Chasis, 1993) the erythrocyte cytoplasm becomes a primary determinant of cellular deformability (Mohandas et al., 1979).

The erythrocyte membrane is a layered structure comprising the lipid bilayer and the membrane skeleton. The lipid bilayer is often considered a two-dimensional incompressible structure without shear resistance, whereas the underlying membrane skeleton is composed of a spectrin network that enables the erythrocyte membrane to resist shear loads (Dimitrakopoulos, 2012). The biconcave discoid shape of a healthy erythrocyte allows it to undergo large deformation of up to 230% of its original dimension while maintaining minimal areal membrane strain.

An erythrocyte has a volume of 94.5 μm^3 and a surface area of 135.2 μm^2 (Li et al., 2014). Compared to the surface area of a sphere with an identical volume, i.e. 98 μm^2, the erythrocyte's discoid shape increases its surface area by approximately 37 μm^2, which is approximately 4.6 times the surface area of a merozoite of 8.0 μm^2 (Dasgupta et al., 2014). This excess surface area suggests that the erythrocyte may wrap the merozoite entirely with a small areal strain in the membrane.

2.2 Merozoite geometry

The idealised ellipsoidal geometry of the merozoite is defined by:

$$(x^2 + y^2 + z^2)^2 = R_a x^3 + (R_a - R_b) x (y^2 + z^2) , \quad (1)$$

where R_a = 1 µm and R_b = 0.7 µm are shape parameters determining the size of the merozoite (Figure 1 a).

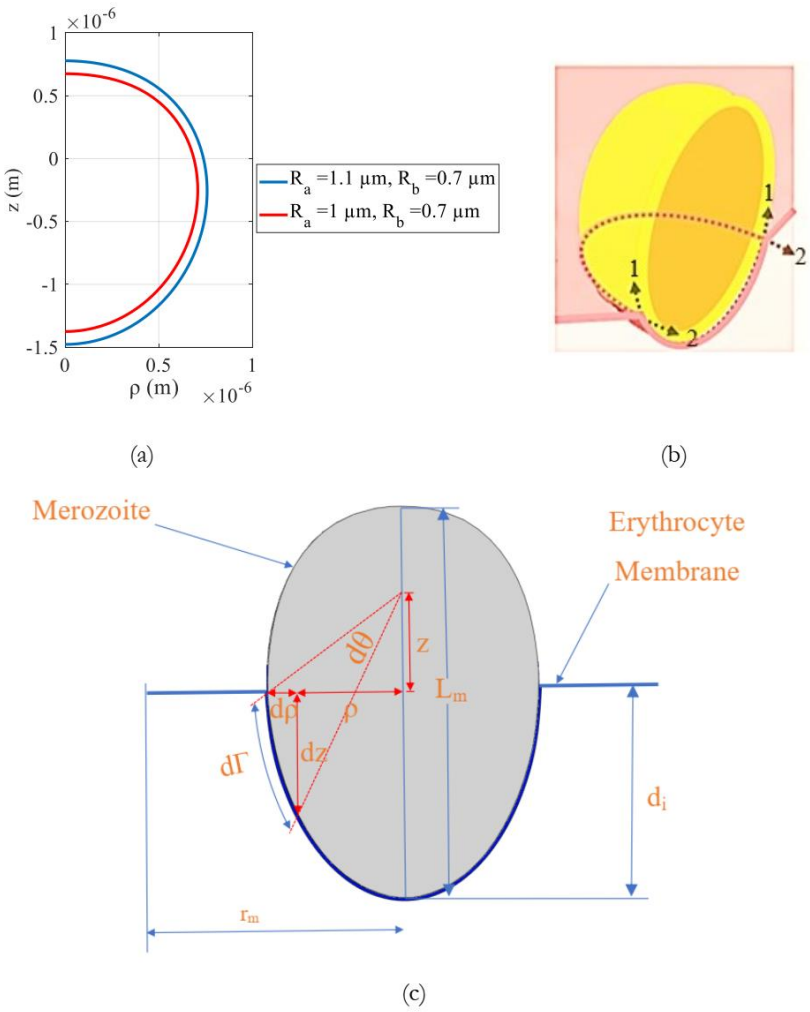

Figure 1: (a) Idealised merozoite shape with geometrical alteration resulting from altering R_a from 1 to 1.1 µm. (b) Principal stretch directions of the erythrocyte membrane, where 1 and 2 represent the meridian and circumferential directions, respectively. (c) An idealised schematic of merozoite partially wrapped by the erythrocyte membrane wrapping mechanism with L_m as total merozoite length and d_i as merozoite indentation depth.

Using spherical coordinate parameterisation, the x, y, and z coordinates of the surface of the merozoite are expressed as (Dasgupta et al., 2014):

$$z(\theta) = (1 + \cos\theta)\,[\,2R_a - R_b(1 - \cos\theta)\,]/4 \tag{2}$$

$$x(\theta, \varphi) = \sin\theta \cos\varphi\,[\,2R_a - R_b(1 - \cos\theta)\,]/4 \tag{3}$$

$$y(\theta, \varphi) = \sin\theta \sin\varphi\,[2R_a - R_b(1 - \cos\theta)\,]/4 \tag{4}$$

where θ and φ are polar angles.

The arc length on the egg-shaped merozoite surface is defined using the first fundamental form:

$$d\Gamma_c^2 = \check{E}\, d\varphi^2 + 2\, \check{A}\, d\varphi\, d\theta + d\theta^2 \tag{5}$$

where $\check{E} = r_\varphi \times r_\varphi$, $\check{A} = r_\theta \times r_\varphi$, $\check{G} = r_\theta \times r_\theta$

$$r_\theta = \frac{\partial x}{\partial \theta}\, i + \frac{\partial y}{\partial \theta}\, j + \frac{\partial z}{\partial \theta}\, k \tag{6}$$

$$r_\varphi = \frac{\partial x}{\partial \varphi}\, i + \frac{\partial y}{\partial \varphi}\, j + \frac{\partial z}{\partial \varphi}\, k \tag{7}$$

Letting $\rho^2 = (x^2 + y^2)$, the matrix of coefficients of the first form is defined:

$$\begin{bmatrix} \check{E} & \check{A} \\ \check{A} & \check{G} \end{bmatrix} = \begin{bmatrix} \rho^2 & \rho\rho' \,(\sin(\varphi - \theta)) \\ \rho\rho'(\sin(\varphi - \theta)) & \rho'^2 + z'^2 \end{bmatrix} \tag{8}$$

where a single prime represents the first partial derivative with respect to θ.

2.3 Deformation of erythrocyte membrane during merozoite wrapping

The erythrocyte membrane is assumed to be flat during the initial contact with the merozoite. During the wrapping of the merozoite, the main erythrocyte membrane strains and stresses are in the meridian and circumferential direction (Figure 1 b), and the erythrocyte membrane deformation is parameterised using the merozoite's shape parameters (Figure 1 c). The shape parameters R_a and R_b can be used to investigate the impact of shape changes of the merozoite on its invasion efficiency.

The erythrocyte membrane deformations are described by meridian and circumferential stretch as follows:

$$\lambda_1 = 1 + (\Gamma - \rho) / r_m \tag{9}$$

$$\lambda_2 = m\left(\rho / \rho_0\right)^n + c \tag{10}$$

with

$$\Gamma = \int_0^{\pi} \sqrt{\rho'^2 + z'^2}\, d\theta \tag{11}$$

Here, ρ and z are the Cartesian coordinates of locations on the surface of the rigid merozoite; m, n, and c determine the magnitude of the principal erythrocyte membrane stretches, and Γ is the coverage length of the erythrocyte membrane on the merozoite surface in the meridian direction. (The subscripts 1 and 2 refer to the erythrocyte membrane's meridian and circumferential principal directions, respectively, see Figure 1b.)

The meridian and circumferential deformation gradients are represented with the derivative of Eqns. (9) and (10):

$$\lambda_1' = \left(\sqrt{\rho'^2 + z'^2} - \rho'\right)/r_m \tag{12}$$

$$\lambda_2' = n\,\rho'\,(\lambda_2 - c)/\rho \tag{13}$$

The local erythrocyte membrane bending is characterised by two principal curvatures, k_1 and k_2:

$$k_1 = z'\,\rho'' - z''\,\rho' / \left(\sqrt{z'^2 + \rho'^2}\right)^3 \tag{14}$$

$$k_2 = 1/\rho \tag{15}$$

where the single and double prime represent the first and second partial derivatives with respect to θ.

2.4 Constitutive law of erythrocyte membrane

A typical erythrocyte model often comprises a Newtonian liquid cytoplasm surrounded by a thin membrane with a thickness of 0.01 μm (Hochmuth et al., 1973). The erythrocyte membrane is considered a mechanically isotropic, incompressible and hyperelastic solid (Villaggio, 1997).

The merozoite-induced erythrocyte membrane dissociation is represented by reducing the erythrocyte elastic modulus from 1 kPa to 0.5 kPa. The Mooney Rivlin strain energy density function per reference volume (Skalak et al., 1973) is:

$$\psi = C_{10}\,(I_1 - 3) + C_{01}\,(I_2 - 3) \tag{16}$$

where C_{10} and C_{01} are empirical material parameters, I_1 and I_2 are the first and second strain invariants related to the principal stretch λ_1 and λ_2 by:

$$I_1 = \lambda_1^2 + \lambda_2^2 + \lambda_1^{-2}\,\lambda_2^{-2} \tag{17}$$

$$I_2 = \lambda_1^{-2} + \lambda_2^{-2} + \lambda_1^2\,\lambda_2^2 \tag{18}$$

The material parameter C_{10} is related to the elastic modulus E of the erythrocyte membrane (Zhang and Zhang, 2011):

$$C_{10} = E/6\,(\,1 + \beta\,) \tag{19}$$

where β ranges from 0 to 0.5. The elastic modulus E is of the order 1 kPa (Hochmuth et al., 1973) and the ratio of two Mooney Rivlin material parameters is $\beta = C_{10}/C_{01} = 0.1$ (Zhang and Zhang, 2011).

The erythrocyte membrane constitutive law is defined by:

$$\sigma_i = \lambda_i\, d\psi/d\lambda_i \tag{20}$$

$$T_i = h_t\, \sigma_i/\,\lambda_1\,\lambda_2 \tag{21}$$

$$T_1 = 2\,h_t\big(\,\lambda_1\,\lambda_2^{-1} - \lambda_1^{-3}\,\lambda_2^{-3}\,\big)\,\big(\partial\psi/\,\partial I_1 + \lambda_2^{2}\,\partial\psi/\,\partial I_2\big) \tag{22}$$

$$T_2 = 2\,h_t\big(\,\lambda_2\,\lambda_1^{-1} - \lambda_1^{-3}\,\lambda_2^{-3}\,\big)\,\big(\partial\psi/\,\partial I_1 + \lambda_1^{2}\,\partial\psi/\,\partial I_2\big) \tag{23}$$

where $h_t = 0.01$ µm is the thickness of the erythrocyte membrane (Hochmuth et al., 1973).

The shear modulus G_s of the erythrocyte membrane is determined by:

$$G_s = \frac{\mu_s}{e_s} \tag{24}$$

with

$$\mu_s = \frac{T_1 - T_2}{2} \tag{25}$$

$$e_s = \frac{\lambda_1^2 - \lambda_2^2}{4} \tag{26}$$

The areal strain A_s of the erythrocyte membrane is expressed by:

$$A_s = (\lambda_1 \lambda_2 - 1) \tag{27}$$

2.5 Equilibrium equations of erythrocyte membrane

For the contact region between the erythrocyte membrane and the rigid merozoite, the equilibrium equations are:

$$\lambda_1^{'} \, dT_1/d\lambda_1 + \lambda_2^{'} dT_1/d\lambda_2 = \rho^{'} \, (T_2 - T_1)/\rho, \tag{28}$$

$$k_1 \, T_1 + k_2 \, T_2 = P \, , \tag{29}$$

where P is the pressure exerted by the merozoite on the erythrocyte membrane surface that is directed normal to the erythrocyte membrane surface. The merozoite wrapping force F_w acting on the erythrocyte membrane surface and causing the erythrocyte membrane to wrap the merozoite is:

$$F_w = P \, A_w \, , \tag{30}$$

where A_w is the surface area of the merozoite wrapped by the erythrocyte membrane:

$$A_w = \int_0^{\pi} \int_0^{2\pi} \sqrt{\check{E} \, \check{G} - \check{A}^2} \, d\theta \, d\varphi. \tag{31}$$

The total indentation force of the merozoite is:

$$F_i = P \, A_p, \tag{32}$$

where A_p is the projected surface area of the erythrocyte membrane:

$$A_p = \pi \, \rho^2.$$

The indentation work, which is the energy required by the parasite to invade a human erythrocyte, is:

$$E_i = F_i\, d_i. \tag{33}$$

where d_i = (max(z) + z) is the indentation depth.

2.6 Governing equations of erythrocyte membrane

The governing differential equations for the contact region are:

$$\lambda_1' = z' \left(\frac{g_3 - n\, g_2\, (\lambda_2 - c)}{2\, r_m\, g_1\, \varrho + g_3\, r_m^2 - n\, g_2\, r_m^2\, (\lambda_2 - c)} \right)^{0.5} \tag{34}$$

$$\lambda_2' = n\, \rho'(\lambda_2 - c) / \rho \tag{35}$$

with

$$g_1(\lambda_1, \lambda_2, \theta) = \frac{dT_1}{d\lambda_1},\ g_2(\lambda_1, \lambda_2, \theta) = \frac{dT_2}{d\lambda_2},\ g_3(\lambda_1, \lambda_2, \theta) = T_1 - T_2.$$

The coverage area of the erythrocyte membrane at each invasion step is:

$$M_c = \frac{100 \left(\int_0^{\pi} \int_0^{2\pi} \sqrt{\check{E}\check{G} - A^2}\, d\theta d\varphi \right)}{A_0}, \tag{36}$$

where A_0 is the total surface area of the merozoite.

With the parameter values in Table 1, the solution of the governing equations can be obtained.

Table 1: Erythrocyte membrane parameters for simulating merozoite wrapping with small and large maximum areal membrane strain of $A_{s,max}$ = 4% and 51%.

$A_{s,max}$ (%)	**E (kPa)**	**C_{10} (Pa)**	**C_{01} (Pa)**	**r_m (μm)**	**c**	**n**	**λ_o**
4	1	183	18.3	50	1	1	1
51	1	183	18.3	4	1	1	1

2.7 Contribution of tight junction, erythrocyte membrane wrapping, and erythrocyte membrane damage to invasion energetics

The tight junction forms a mechanical link between the merozoite and erythrocyte membrane to facilitate membrane wrapping. It acts as an anchor location where the merozoite's actomyosin motors pull the erythrocyte membrane. The tight junction is assumed to exert tension in the circumferential direction at any equilibrium point. In the erythrocyte membrane, a tension acting in the meridian direction is assumed to resist the forces applied by the merozoite. The tensions in meridian direction T_1 and circumferential direction T_2 are used to describe the energetics of the tight junction and the erythrocyte membrane. The parameter values in Table 1 consider the contributions of the tight junction and the erythrocyte membrane wrapping during small and large strain deformation of the erythrocyte membrane.

After attaching to the erythrocyte, the merozoite induces phosphorylation that locally dissolves the spectrin network, forming the erythrocyte membrane's skeleton. This process changes the erythrocyte membrane's mechanical properties (Zuccala and Baum, 2011). For example, phosphorylation of band 4.1 weakens the connections between band 4.1, spectrin and actin, which leads to membrane destabilisation (Betz et al., 2009). The phosphorylation of β spectrin also leads to decreased membrane stability (Manno et al., 1995); tyrosine phosphorylation of the SLC4A1 protein weakens the attachment of SLC4A1 to the underlying spectrin network and increases the membrane mobility by altering ankyrin binding (Ferru et al., 2011). To assess the impact of membrane damage, the erythrocyte membrane elastic modulus was reduced from 1 kPa to 0.5 kPa.

3 Results

The developed model was applied to simulate the wrapping by an erythrocyte membrane. Two cases of maximum erythrocyte membrane areal strain were considered, i.e. (i) $A_{s,max}$ = 4% as a generally accepted upper threshold for initiation of cell lysis during quasi-static deformation of the membrane (Li et al., 2013), and (ii) $A_{s,max}$ = 51% to investigate larger deformations with an upper threshold of 40% yield areal strain of the erythrocyte membrane (Li et al., 2013). The effect of local membrane damage due to phosphorylation by the

merozoite was considered by reducing the erythrocyte membrane's elastic modulus from 1 kPa to 0.5 kPa.

The maximum areal strain in the erythrocyte membrane during merozoite wrapping was implemented with a large circular membrane section with radius r_m = 50 µm for $A_{s,max}$ = 4% and a small membrane section with r_m = 4 µm for $A_{s,max}$ = 51%, along with the parameter values specified in Table 1.

The merozoite wrapping with $A_{s,max}$ = 4% induced maximum principal stretches of $\lambda_{1,max}$ = 1.04 in the meridian direction and $\lambda_{2,max}$ = 1.000046 in circumferential direction of the erythrocyte membrane (Figure 2). The maximum circumferential stretch $\lambda_{2,max}$ occurred at a meridian stretch of λ_1 = 1 (Figure 2 a). Permitting a higher areal membrane strain of $A_{s,max}$ = 51% during merozoite wrapping resulted in a substantially increased maximum principal membrane stretches of $\lambda_{1,max}$ = 1.5 and $\lambda_{2,max}$ = 1.0375, the latter occurring at λ_1 = 1.26 (Figure 2 b). The circumferential and meridian stretch in the erythrocyte membrane during the invasion process is illustrated in (Figure 2 c-f).

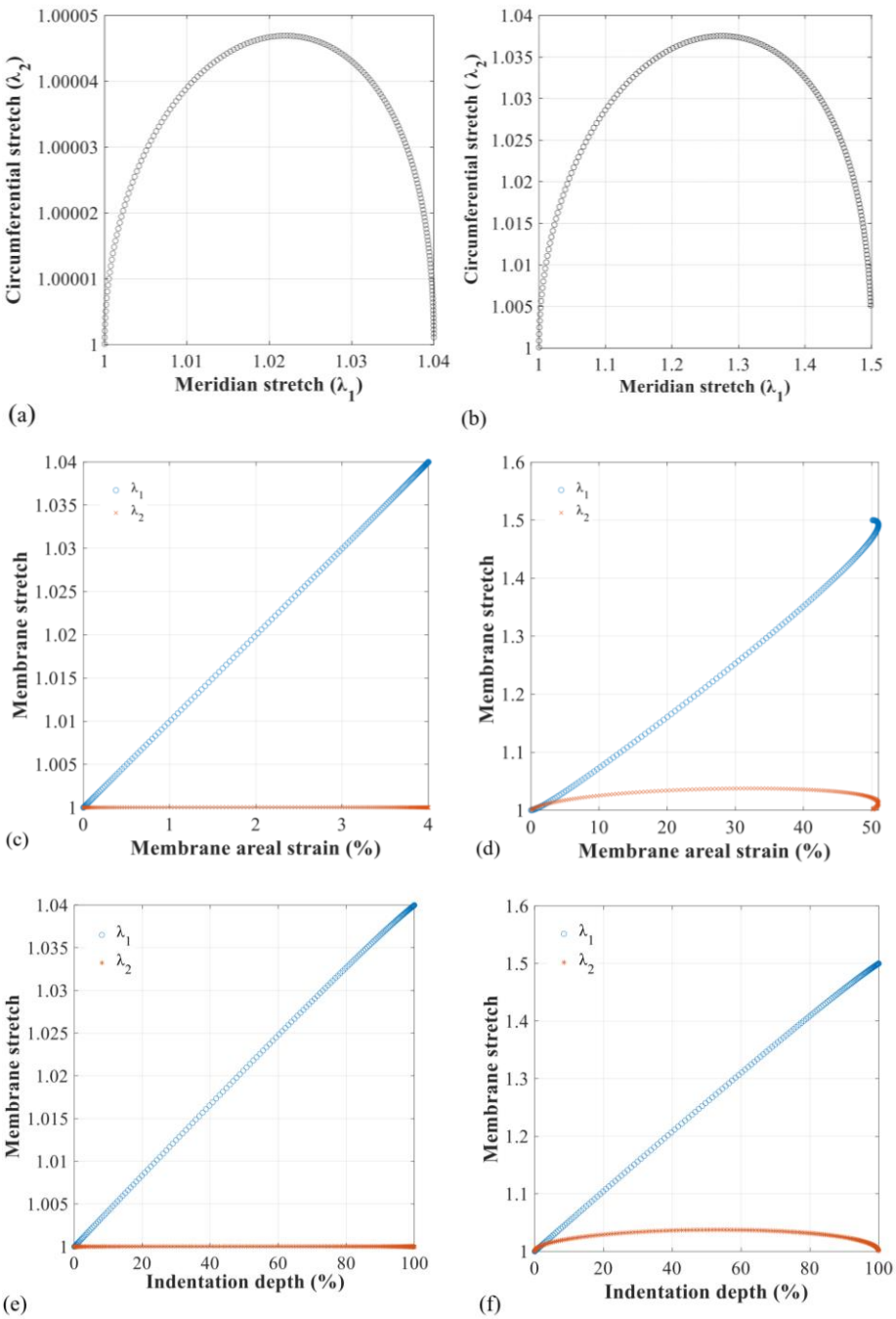

Figure 2: Numerical solution of principal stretches in the erythrocyte membrane for the complete wrapping of the merozoite. Circumferential stretch λ_2 versus meridian stretch λ_1 for (a) small maximum areal strain of $A_{s,max}$ = 4% and (b) large maximum areal strain of $A_{s,max}$ = 51%. The meridian stretch λ_1 and circumferential stretch λ_2 versus areal strain in the erythrocyte membrane for $A_{s,max}$ = 4% (c) and 51% (d). The meridian stretch λ_1 and circumferential stretch λ_2 versus indentation depth normalised to merozoite length L_m for $A_{s,max}$ = 4% (e) and 51% (f).

The tension induced by the circumferential and meridian stretches for small areal strain up to $A_{s,max}$ = 4% reflects a near-linear constitutive response of the erythrocyte membrane (Figure 3 a). For large areal strain, $A_{s,max}$ = 51%, the erythrocyte membrane's non-linear elastic response with strain softening is apparent (Figure 3 b).

The model's prediction of the non-dimensional meridian membrane tension T_1 agrees better with Hooke's law non-dimensional tension than the Mooney-Rivlin-based non-dimensional tension for small membrance deformation with $A_{s,max}$ = 4% (Omori et al., 2011) (Figure 3 a, c), and for larger membrane strain with $A_{s,max}$ = 51 (Figure 3 b, d).

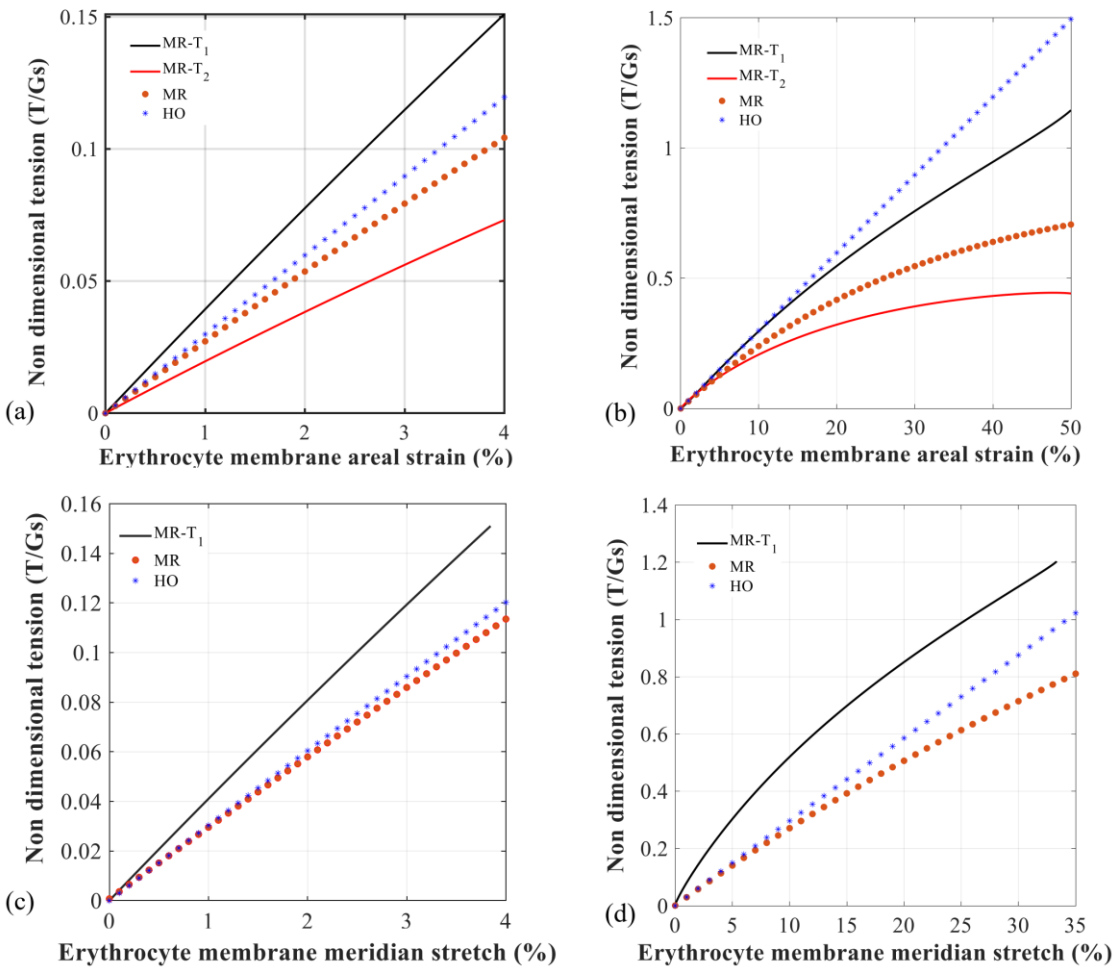

Figure 3: Non-dimensional isotropic principal tension versus areal strain (a, b) and meridian strain (c, d) in the erythrocyte membrane during merozoite wrapping for the maximum areal strain of $A_{s,max}$ = 4% (a, c) and 51% (b, d). Solutions for the meridian (MR-T_1) and circumferential tension (MR-T_2) obtained with the developed Mooney-Rivlin-based erythrocyte membrane constitutive model (Eqns. (22) and (23)) compared to solutions of non-dimensional tension based on the linear elastic Hooke's law (HO) and the non-linear

elastic Mooney-Rivlin law (MR) from Omori et al. (2011).

The erythrocyte membrane's strain softening was also apparent by a decreasing shear modulus with increasing areal strain (Figure 4 a**)**. The meridian and circumferential membrane stresses associated with an areal strain of $A_{s,max}$ = 4% were σ_1 = 63.1 Pa and σ_2 = 30.5 Pa (see Figure 4 b).

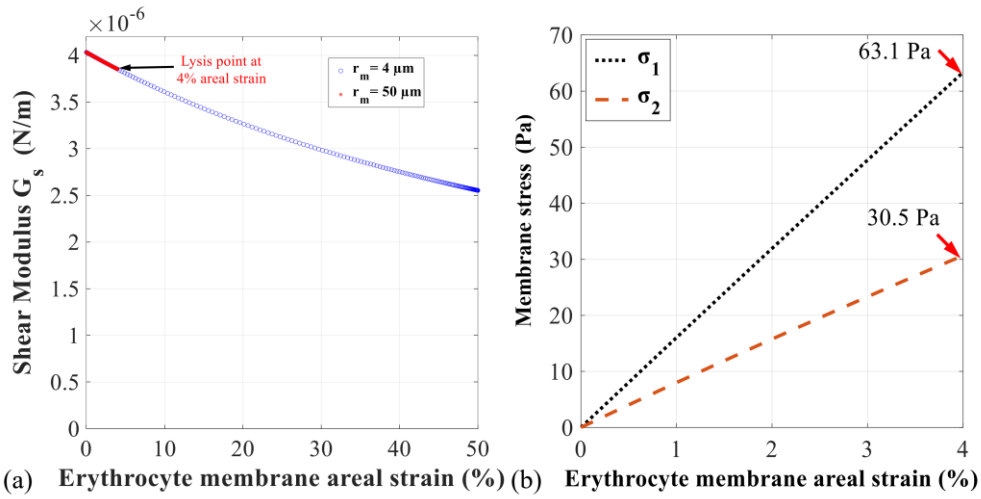

Figure 4: (a) Shear modulus versus areal strain of the erythrocyte membrane during complete wrapping of the merozoite. The decrease of the shear modulus with increasing areal strain represents strain softening. (b) Meridian and circumferential stress versus areal strain in the erythrocyte membrane during complete merozoite wrapping. The stress associated with the assumed lysis threshold of the areal strain of $A_{s,max}$ = 4% is σ_1 = 63.1 Pa in meridian and σ_2 = 30.5 Pa in the circumferential direction.

The total indentation force F_i during membrane wrapping was predicted to increase nearly linearly up to a normalised indentation depth of 85.2% marking the position of the merozoite's maximum diameter and decrease after that. The indentation force was higher for the large ($A_{s,max}$ = 51%) than the small membrane strain ($A_{s,max}$ = 4%); however, the F_i maximum occurred at the same indentation depth (see Figure 5 a). The total wrapping force was predicted to increase exponential during the late stages of the invasion process. These results illustrate that a large surface area of the erythrocyte membrane involved in the wrapping leads to smaller magnitudes of total wrapping and indentation forces.

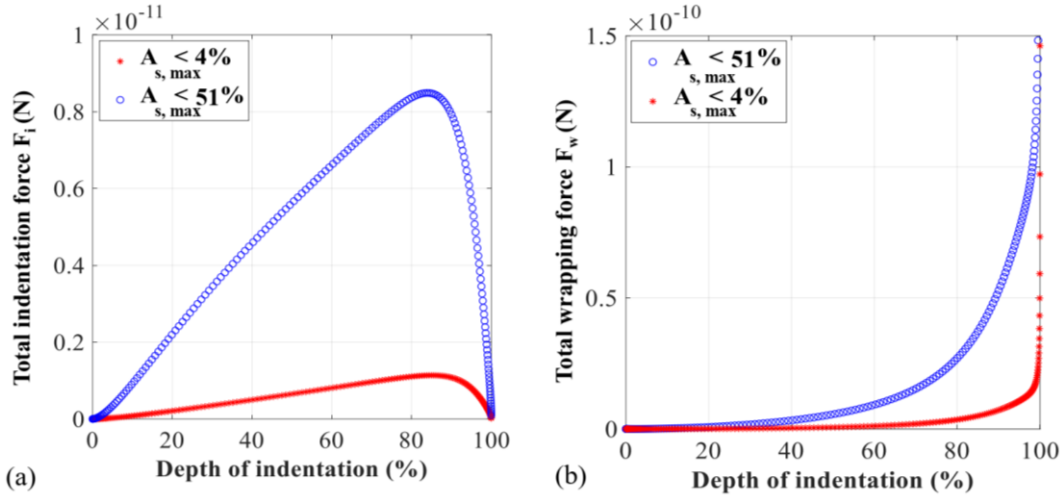

Figure 5. Forces involved in merozoite wrapping versus normalised indentation depth d_i/L_m for small ($A_{s,max}$ = 4%) and large maximum areal strain ($A_{s,max}$ = 51%) in the erythrocyte membrane. (a) Total indentation force F_I acting in the direction of the merozoite's long axis. (b) Total wrapping force F_W acting normal to the surface of the merozoite.

The total indentation work E_i required by the merozoite to overcome the barrier energy of the erythrocyte membrane was predicted to increase with increasing indentation depth. E_i reaches a maximum of $E_i = 1.92\times10^{-18}$ J for $A_{s,max}$ = 4% and $E_i = 1.40\times10^{-17}$ J for $A_{s,max}$ = 51% at the same normalised indentation depth as the total indentation force, i.e. at 85.2% (Figure 6). A reduction of the erythrocyte membrane's elastic modulus from 1 to 0.5 kPa to simulate weakening due to phosphorylation of the spectrin network led to a reduction of the total indentation work by 50% to $E_i = 0.97\times10^{-18}$ J for $A_{s,max}$ = 4% and $E_i = 0.70\times10^{-17}$ J for $A_{s,max}$ = 51% (Figure 6).

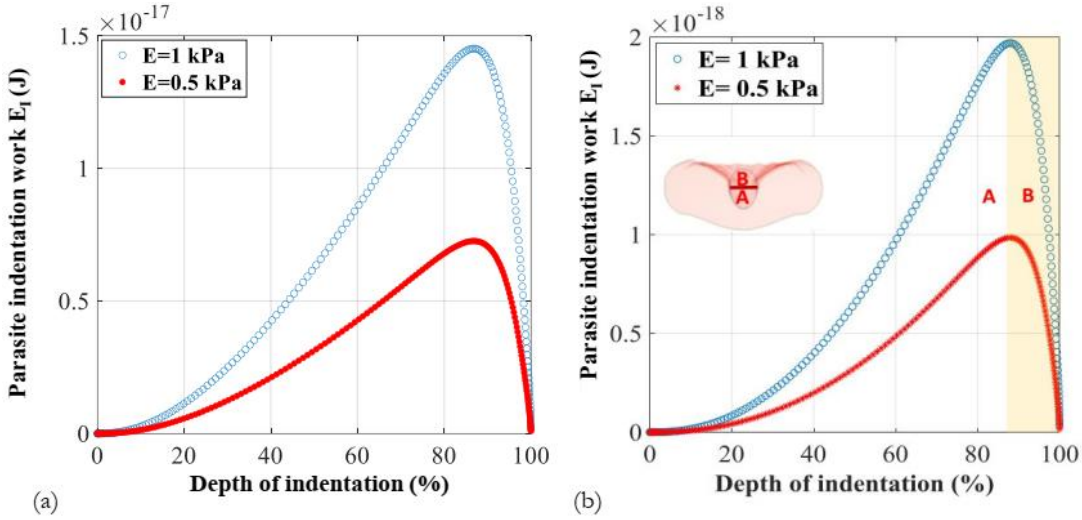

Figure 6: Indentation work E_i required for merozoite wrapping versus normalised indentation depth d_i/L_M without and with phosphorylation of the spectrin network (represented by reducing the membrane's elastic modulus from 1 kPa to 0.5 kPa) for $A_{s,max}$ = 51% (a) and 4 % (b). Phosphorylation decreased E_i by 50%. In (b), labels A and B represent the indentation depth regions for which the merozoite and tight junction, respectively, provide the indentation energy, with the change occurring at a normalised indentation depth of 85.2%.

4 Discussion

An analytical model for wrapping a malaria merozoite by an erythrocyte was developed. The effects of the erythrocyte membrane area available for wrapping, membrane damage through phosphorylation of the spectrin network, and the tight junction between merozoite and erythrocyte membrane in the invasion mechanics were investigated. The tight junction was defined by a line tension acting in the circumferential direction of the erythrocyte membrane with an initial radius ρ_o. The total energy required for a successful invasion was determined by computing the total work done by the merozoite that represents the contribution of the tight junction and the erythrocyte membrane.

The results of the developed analytical model indicate that during the early stage of active invasion, the work done by the merozoite increases progressively and is stored as internal energy in the tight junction and the erythrocyte membrane. This energy is utilised during the late phase of the invasion, facilitating the sealing of the erythrocyte membrane during the late invasion stage.

Two erythrocyte membrane wrapping cases were assessed, distinguished by the maximum areal strain permitted in the erythrocyte membrane during the invasion, namely $A_{s,max}$ = 4% and 51%. The strain limits were implemented with circular erythrocyte membrane areas of different sizes involved in the wrapping; a large area with r_m = 50 µm for the small strain limit and a small area with r_m = 4 µm for the large strain limit. It was observed in the predictions that the merozoite wrapping force F_w and the total indentation force F_i were lower for low areal strain in the erythrocyte membrane (and large wrapping membrane area) than for the large strain (and small membrane area) (Figure 5). This finding suggests that the merozoite's invasiveness efficiency depends on the size of the erythrocyte membrane available and the areal strain induced in the membrane during the wrapping process.

It has been reported that discoid-shaped erythrocytes are more deformable than ellipsoidal or spherical erythrocytes, often found with hereditary disorders such as elliptocytosis and spherocytosis (Li et al., 2018). The increased deformability stems from the discoid's larger surface-to-volume ratio (S/V) than the spherical and elliptic shapes (Tomaiuolo, 2014). However, it has been unclear whether and how the different erythrocyte shapes affect the invasion of merozoites. Predictions with the developed model revealed that the required invasion force and energy are lower for a large erythrocyte membrane area than for a small membrane area involved in the wrapping interaction (Figure 5). The lower invasion force and energy may promote the merozoite invasion and increase invasion efficiency. This finding can also partly explain why individuals with abnormal erythrocyte shapes, e.g., caused by spherocytosis, elliptocytosis, and sickle cell anaemia, are less susceptible to malaria. However, further analysis is needed to quantify the impact of surface to volume ratio on the merozoite invasiveness.

The effect of merozoite-induced phosphorylation of the erythrocyte's spectrin network and membrane damage in the invasion mechanics was assessed by reducing the elastic modulus of the erythrocyte membrane in the Mooney Rivlin law from 1 kPa for the intact membrane to 0.5 kPa for the membrane with damage. This change led to a decrease in the required invasion work and energy (Figure 6), suggesting that the phosphorylation of the erythrocyte membrane supports the merozoite invasion and increases invasion efficiency.

The mechanical erythrocyte membrane response in the meridian direction predicted by the developed model agrees better with the the solution based on Hooke's law than original Mooney-Rivlin model (Omori et al., 2011). The noticeable differences between the

developed model's predictions and the previous numerical data are due to the different loading modes, i.e. merozoite-induced stretch for the developed model versus biaxial stretch for the Hooke's law and Mooney-Rivlin solutions by Omori et al. (2011) (Figure 3).

The developed analytical model has limitations, i.e. the restriction to 2D analysis, the absence of the erythrocyte cytoplasm, and the lack of experimental data for calibration and validation. Extending the model is recommended for future work.

5 Conclusions

The developed analytic model is the first capable of predicting the invagination forces and energetics generated by the merozoite actomyosin machinery and erythrocyte membrane and assessing the merozoite's invasiveness based on the erythrocyte membrane's shape and mechanics. The current study demonstrated the model's feasibility to provide new knowledge on the physical mechanisms of the merozoite invasion process that contribute to the invasion efficiency and may, especially after extension in the future, be beneficial in the discovery of new invasion-blocking anti-malaria drugs.

Funding

This research was supported financially by the National Research Foundation of South Africa (grants CPRR14071676206 and IFR14011761118 to TF) and the South African Medical Research Council (grant SIR328148 to TF), and grants from the World Bank to the University of Malawi. The funders had no role in study design, data collection and analysis, decision to publish, or preparation of the manuscript. Any opinion, findings, conclusions, or recommendations expressed in this publication are those of the authors and do not necessarily represent the official views of the funding agencies.

Conflict of Interests

The authors declare no conflict of interest.

Data availability

Data supporting the results presented in this article are available on the University of Cape Town's institutional data repository (ZivaHub) under https://doi.org/10.25375/uct.19641306 as Msosa C, Abdalrahman T, Franz T. Data for an analytical model describing the mechanics

of erythrocyte membrane wrapping during active invasion of a plasmodium falciparum merozoite, Cape Town, ZivaHub, 2022, DOI 10.25375/uct.19641306.

References

Abdalrahman, T., Franz, T., 2017. Analytical modeling of the mechanics of early invasion of a merozoite into a human erythrocyte. Journal of biological physics 43, 471-479.

Betz, T., Lenz, M., Joanny, J.F., Sykes, C., 2009. ATP-dependent mechanics of red blood cells. Proceedings of the National Academy of Sciences of the United States of America 106, 15320-15325.

Cowman, A.F., Crabb, B.S., 2006. Invasion of red blood cells by malaria parasites. Cell 124, 755-766.

Dasgupta, S., Auth, T., Gov, N.S., Satchwell, T.J., Hanssen, E., Zuccala, E.S., Riglar, D.T., Toye, A.M., Betz, T., Baum, J., Gompper, G., 2014. Membrane-Wrapping Contributions to Malaria Parasite Invasion of the Human Erythrocyte. Biophysical Journal 107, 43-54.

Dimitrakopoulos, P., 2012. Analysis of the variation in the determination of the shear modulus of the erythrocyte membrane: Effects of the constitutive law and membrane modeling. Physical review. E, Statistical, nonlinear, and soft matter physics 85, 041917-041917.

Ferru, E., Giger, K., Pantaleo, A., Campanella, E., Grey, J., Ritchie, K., Vono, R., Turrini, F., Low, P.S., 2011. Regulation of membrane-cytoskeletal interactions by tyrosine phosphorylation of erythrocyte band 3. Blood 117, 5998-6006.

Guiguemde, W.A., Shelat, A.A., Bouck, D., Duffy, S., Crowther, G.J., Davis, P.H., Smithson, D.C., Connelly, M., Clark, J., Zhu, F., Jiménez-Díaz, M.B., Martinez, M.S., Wilson, E.B., Tripathi, A.K., Gut, J., Sharlow, E.R., Bathurst, I., El Mazouni, F., Fowble, J.W., Forquer, I., McGinley, P.L., Castro, S., Angulo-Barturen, I., Ferrer, S., Rosenthal, P.J., DeRisi, J.L., Sullivan, D.J., Lazo, J.S., Roos, D.S., Riscoe, M.K., Phillips, M.A., Rathod, P.K., Van Voorhis, W.C., Avery, V.M., Guy, R.K., 2010. Chemical genetics of Plasmodium falciparum. Nature 465, 311-315.

Hochmuth, R.M., Mohandas, N., Blackshear, P.L., 1973. Measurement of the Elastic Modulus for Red Cell Membrane Using a Fluid Mechanical Technique. Biophysical Journal 13, 747-762.

Li, F., Chan, C.U., Ohl, C.D., 2013. Yield strength of human erythrocyte membranes to impulsive stretching. Biophysical Journal 105, 872-879.

Li, H., Lu, L., Li, X., Buffet, P.A., Dao, M., Karniadakis, G.E., Suresh, S., 2018. Mechanics of diseased red blood cells in human spleen and consequences for hereditary blood disorders. Proceedings of the National Academy of Sciences 115, 9574-9579.

Li, X., Peng, Z., Lei, H., Dao, M., Karniadakis, G.E., 2014. Probing red blood cell mechanics, rheology and dynamics with a two-component multi-scale model. Philosophical Transaction A: Mathematical, Physical and Engeering Sciences 372.

Manno, S., Takakuwa, Y., Nagao, K., Mohandas, N., 1995. Modulation of erythrocyte membrane mechanical function by beta-spectrin phosphorylation and dephosphorylation. Journal of Biological Chemistry 270, 5659-5665.

Mohandas, N., Chasis, J.A., 1993. Red blood cell deformability, membrane material properties and shape: regulation by transmembrane, skeletal and cytosolic proteins and lipids. Seminars in hematology 30, 171-192.

Mohandas, N., Phillips, W.M., Bessis, M., 1979. Red blood cell deformability and hemolytic anemias. Seminars in hematology 16, 95-114.

Omori, T., Ishikawa, T., Barthès-Biesel, D., Salsac, A.V., Walter, J., Imai, Y., Yamaguchi, T., 2011. Comparison between spring network models and continuum constitutive laws: application to the large deformation of a capsule in shear flow. Physical review. E, Statistical, nonlinear, and soft matter physics 83, 041918.

Plouffe, D., Brinker, A., McNamara, C., Henson, K., Kato, N., Kuhen, K., Nagle, A., Adrián, F., Matzen, J.T., Anderson, P., Nam, T.-g., Gray, N.S., Chatterjee, A., Janes, J., Yan, S.F., Trager, R., Caldwell, J.S., Schultz, P.G., Zhou, Y., Winzeler, E.A., 2008. In silico activity profiling reveals the mechanism of action of antimalarials discovered in a high-throughput screen. Proceedings of the National Academy of Sciences of the United States of America 105, 9059-9064.

Qi, D., Kaur Gill, N., Santiskulvong, C., Sifuentes, J., Dorigo, O., Rao, J., Taylor-Harding, B., Ruprecht Wiedemeyer, W., Rowat, A.C., 2015. Screening cell mechanotype by parallel microfiltration. Sci. Rep. 5, 17595.

Rottmann, M., McNamara, C., Yeung, B.K.S., Lee, M.C.S., Zou, B., Russell, B., Seitz, P., Plouffe, D.M., Dharia, N.V., Tan, J., Cohen, S.B., Spencer, K.R., González-Páez, G.E., Lakshminarayana, S.B., Goh, A., Suwanarusk, R., Jegla, T., Schmitt, E.K., Beck, H.-P., Brun, R., Nosten, F., Renia, L., Dartois, V., Keller, T.H., Fidock, D.A., Winzeler, E.A., Diagana, T.T., 2010. Spiroindolones, a new and potent chemotype for the treatment of malaria. Science (New York) 329, 1175-1180.

Skalak, R., Tozeren, A., Zarda, R.P., Chien, S., 1973. Strain Energy Function of Red Blood Cell Membranes. Biophysical Journal 13, 245-264.

Tomaiuolo, G., 2014. Biomechanical properties of red blood cells in health and disease towards microfluidics. Biomicrofluidics 8, 051501.

Villaggio, P., 1997. Mathematical Models for Elastic Structures. Cambridge University Press, Cambridge.

Zhang, Z., Zhang, X., 2011. Mechanical behavior of the erythrocyte in microvessel stenosis. Science China Life Sciences 54, 450-458.

Zuccala, E.S., Baum, J., 2011. Cytoskeletal and membrane remodelling during malaria parasite invasion of the human erythrocyte. British Journal of Haematology 154, 680-689.